Geophysical Research Letters

RESEARCH LETTER
10.1029/2025GL120917

Revealing the Mechanisms of Heat Extremes Using an AI Enabled Diagnostic Framework

Longzhen Xiang[1,2,3], Ya Wang[1,2], Robin T. Clark[4], Kai Yang[5], Gang Huang[1,3], Xichen Li[6], Pengfei Lin[1], Kaiming Hu[1,7], Weichen Tao[8], and Xia Qu[7]

[1]National Key Laboratory of Earth System Numerical Modeling and Application, Institute of Atmospheric Physics, Chinese Academy of Sciences, Beijing, China, [2]Earth System Numerical Simulation Science Center, Institute of Atmospheric Physics, Chinese Academy of Sciences, Beijing, China, [3]University of Chinese Academy of Sciences, Beijing, China, [4]Met Office Hadley Centre, Met Office, Exeter, UK, [5]Commonwealth Scientific and Industrial Research Organisation (CSIRO) Environment, Hobart, TAS, Australia, [6]Institute of Ocean Research, Peking University, Beijing, China, [7]Center for Monsoon System Research, Institute of Atmospheric Physics, Chinese Academy of Sciences, Beijing, China, [8]State Key Laboratory of Numerical Modeling for Atmospheric Sciences and Geophysical Fluid Dynamics, Chinese Academy of Sciences, Beijing, China

Key Points:

- We developed an AI-enabled, prediction based diagnostic framework to globally identify the high impact regions of extreme heatwaves
- The extreme heatwave was influenced by a relay-like sequence of a combination of local and remote drivers
- Prediction with initial anomalies from high impact regions only can well reconstruct the heatwave

Supporting Information:

Supporting Information may be found in the online version of this article.

Correspondence to:

Y. Wang and G. Huang,
wangya@mail.iap.ac.cn;
hg@mail.iap.ac.cn

Citation:

Xiang, L., Wang, Y., Clark, R. T., Yang, K., Huang, G., Li, X., et al. (2026). Revealing the mechanisms of heat extremes using an AI enabled diagnostic framework. *Geophysical Research Letters*, *53*, e2025GL120917. https://doi.org/10.1029/2025GL120917

Received 8 DEC 2025
Accepted 25 MAR 2026

Author Contributions:

Conceptualization: Ya Wang, Kaiming Hu
Formal analysis: Longzhen Xiang
Funding acquisition: Ya Wang, Gang Huang
Investigation: Longzhen Xiang
Methodology: Ya Wang
Project administration: Gang Huang
Supervision: Ya Wang, Gang Huang, Pengfei Lin
Validation: Longzhen Xiang
Visualization: Longzhen Xiang
Writing – original draft: Longzhen Xiang

Abstract Heat extremes have become a major health hazard around the world. Understanding their mechanisms remains a major challenge because the physical drivers interact in a nonlinear way. Here we introduce a globally perturbed reforecast framework driven by the Neural general circulation model (NeuralGCM). Sensitivity reforecast experiments that independently remove initial condition anomalies over spatially distinct patches identified the high impact regions (HIRs) for the record-breaking August 2022 South China heatwave (SCH22) in Europe and North America (NA) through changes in forecast skill, which are further confirmed by dynamic diagnostics. Forecasts initialized using anomalies only from HIRs covering just 25% of the global domain successfully reproduce the evolution and spatial pattern of SCH22. These findings can also generalize to another AI-based weather model FuXi. Our proposed framework helps to improve accessibility to global-scale diagnostic for extreme events with robust results.

Plain Language Summary In August 2022, South China (SC) experienced an extreme heatwave that threatened human health and caused substantial property damage. Here we use an AI weather prediction model NeuralGCM to find globally where are the regions that have the largest impact to the extreme heatwave. NeuralGCM well predicted the extreme high temperature in SC, and the related physical processes like air sinking and cloud feedback. We did 24 groups of sensitivity experiments, and compared to the control prediction to show that, the heatwave was influenced by a relay-like sequence. Local forcings dominated at 0–5 days, European anomalies affected the intermediate stage, and North American anomalies contributes to its intensification. With initial conditions from these high impact regions (HIRs) only, NeuralGCM can well reconstruct the extreme heatwave in SC, and these results can be confirmed by another AI model FuXi.

1. Introduction

Extreme weather events, most notably heatwaves (Domeisen et al., 2023; Stott et al., 2004; Thompson et al., 2023; Zhang et al., 2023) and heavy rainfall (Boers et al., 2019; Dong et al., 2021; Patricola & Wehner, 2018), have become more frequent and intense in recent decades in multiple parts of the world, often with devastating societal, health, and economic impacts (Liang, 2022; Seneviratne et al., 2023; Smiley et al., 2022). Robust and clear understanding of their possible causes is therefore critical, not only for advancing our science but also for adaptation and decision makers (Bellprat et al., 2019; Hai & Perlman, 2022; Mora et al., 2017; Newman & Noy, 2023). However, it usually requires a far greater focus on individual events, rather than the less focused assessment of general extremes (Blanchard-Wrigglesworth et al., 2023; Leach et al., 2021). This requires reproducing multiple simulations of a specific event to assess uncertainty, whether through statistical analyses, dynamical diagnostics (Xu & Liang, 2020; Zhang et al., 2024; Zheng & Wang, 2021) or targeted sensitivity experiments (Di Capua et al., 2021; Touma et al., 2021; Wang et al., 2021).

One such event requiring a concerted effort occurred in August 2022: an extreme heatwave in South China (SCH22), the most prolonged and intense August heatwave since 1961, with monthly mean 950 hPa and near-

Writing – review & editing: Longzhen Xiang, Ya Wang, Robin T. Clark, Kai Yang, Xichen Li, Pengfei Lin, Kaiming Hu, Weichen Tao, Xia Qu

surface temperatures of 28.3°C and 28.6°C, respectively (Figure 1a), both exceeding an unprecedented two standard deviations above the historical mean and corresponding to return periods of ∼167 and ∼500 years (Figure S1 in Supporting Information S1). During its development phase, anomalies of the daily 950 hPa temperature increased sharply from 2.6°C on August 2nd to approximately 5°C by the 13th (Figure 1b), persisting until the 23rd (Figure S2b in Supporting Information S1). 360 million people experienced daily maximum temperatures above 40°C, and roughly 1.48 million km^2 in China underwent moderate to severe drought, causing economic losses exceeding ¥51.2 billion (Lu et al., 2024; Mallapaty, 2022). Previous studies have linked this event to anthropogenic warming (Gong et al., 2024; Ma et al., 2024), land-atmosphere feedbacks (Fu et al., 2024; Wang et al., 2023), and remote sea surface temperature (SST) anomalies in the Pacific, Indian, and even Atlantic Ocean via Rossby wave trains (Jiang et al., 2023; Ma et al., 2024; Ma et al., 2023; Tang et al., 2023). These studies provided a comprehensive research paradigm by combining statistical methods and model experiments. Nonetheless, such monthly mean, quasi-stationary features alone are insufficient in explaining the rapid intensification. Fundamental questions remain about the precursors heralding such an unusual heatwave. In particular, the relative causative roles of differing parts of the world on specific stages of the event.

To identify the high impact regions (HIRs) of an extreme event, one convincing way is using forecast-based GCM sensitivity experiments to identify the potential roles of specific regions. It inherently preserves causal relationships and avoids the ambiguities of accurately representing a specific extreme event in large ensembles of climate model simulations (Leach et al., 2021; Lin et al., 2022; Pyrina & Domeisen, 2023). Recent advances in artificial intelligence (AI)-driven weather models offer a pathway forward to globally resolving the HIRs (Jiménez-Esteve et al., 2025; Tradowsky et al., 2023; Vonich & Hakim, 2024). While most current AI models are purely data-driven and exhibit physical inconsistencies to some extent, NeuralGCM integrates a differentiable dynamical core with learned physics modules (Kochkov et al., 2024), thereby improving physical fidelity and enhancing the reconstruction of extreme events (Meng et al., 2026). In this study, we propose a reforecast-based framework using NeuralGCM to determine the HIRs of extremes. First, we evaluate the skill of NeuralGCM at reforecasting extreme heatwaves by a control reforecast experiment initialized by observed anomalies. Next, we conduct a suite of regional-conditioned sensitivity experiments to systematically assess their influence on the event's evolution. We identify a set of HIRs that most strongly influence event onset and development, which are subsequently validated in a follow-up reforecast experiment initialized solely with the anomalies in the HIRs. Finally, we perform a dynamical analysis to elucidate the mechanisms that underlie both the local triggering and subsequent remote amplification. A schematic diagram summarizing the AI-model-based prediction framework is shown in Figure S3 of Supporting Information S1.

2. Data and Methods

2.1. Data

Hourly 950 hPa temperature and 200 hPa geopotential fields of August 2022 are obtained from the ERA5 reanalysis (Hersbach et al., 2023a, 2023b) with daily averages calculated at 6-hr intervals. Climatological baselines are monthly means of August spanning from 1981 to 2010. Initial conditions used for inference are from Analysis-Ready, Cloud Optimized (ARCO) ERA5. All data in this study are interpolated onto the 1.4° grid of NeuralGCM for comparison.

2.2. Methods

2.2.1. NeuralGCM Configuration and Control Prediction

Neural general circulation model (NeuralGCM) is a fully differentiable, hybrid atmospheric GCM featuring a differentiable dynamical core for solving the discretized governing dynamical equations and a learned physics module that parameterizes physical processes with a neural network. Pre-trained 1.4° horizontal resolution deterministic checkpoint is used in this study (Kochkov et al., 2024), and we test the robustness of our results based on FuXi cascaded machine learning model (Chen et al., 2023, Text S1 in Supporting Information S1).

The control prediction in this study is initialized at 00:00 UTC on 2nd August 2022, and integrated at 6-hourly timesteps to 18:00 UTC on 16th August 2022. This time period falls entirely outside of the training and evaluation period of NeuralGCM. Results from August 2nd–13th are selected and aggregated to daily means for further analysis.

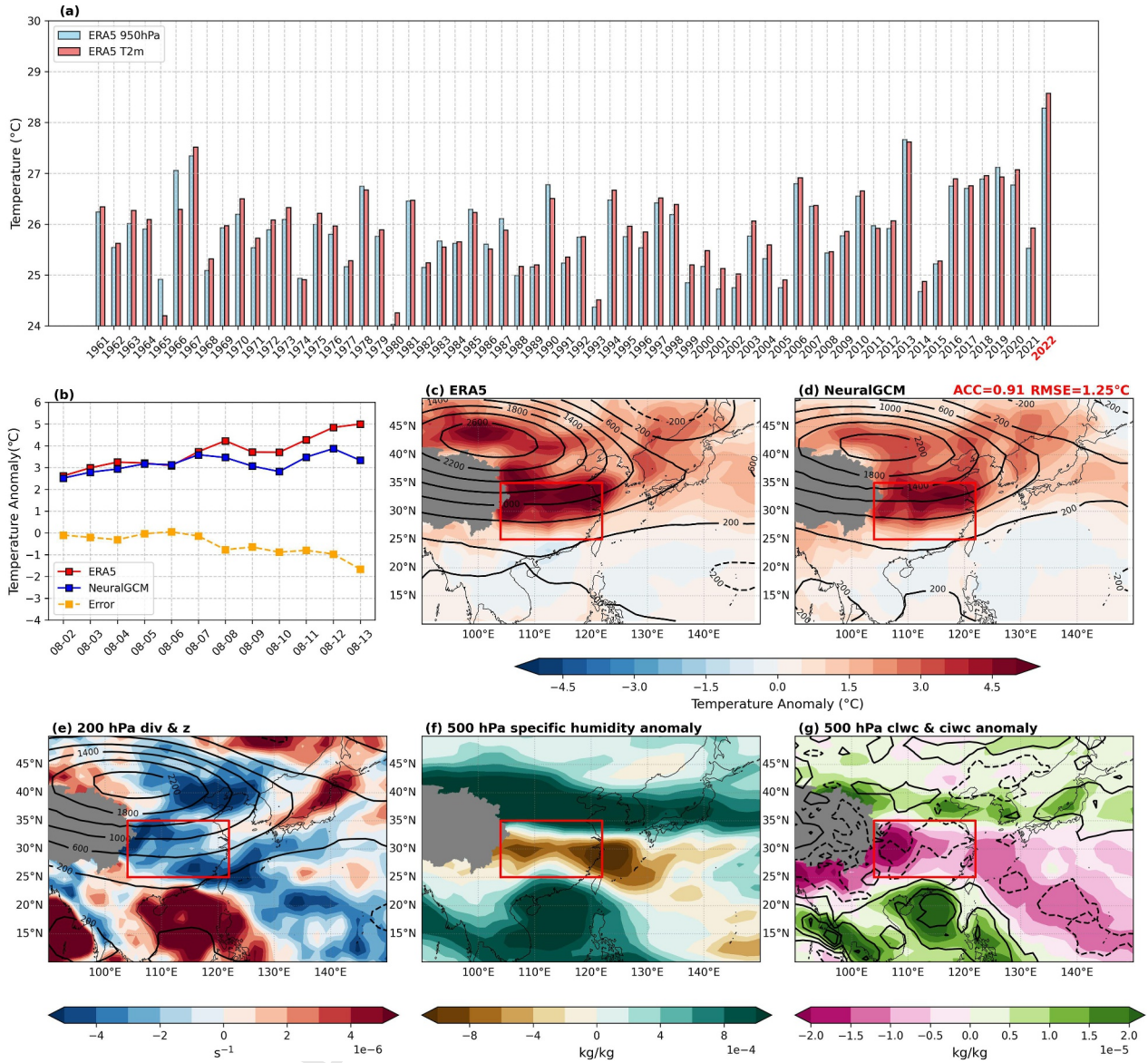

Figure 1. Spatiotemporal features of SCH22 and the NeuralGCM prediction. (a) 1961–2022 SC average temperature in August from ERA5 monthly reanalysis (blue: 950 hPa temperature; red: 2 m surface temperature). (b) 950 hPa temperature anomaly sequence of SC (red boxes in c-g) from ERA5 reanalysis (red) and NeuralGCM prediction (blue). Yellow dashed line is the prediction error. 950 hPa temperature anomaly (shading) and 200 hPa geopotential anomaly (contour) averaged from August 2nd–13th of (c) ERA5 reanalysis and (d) NeuralGCM prediction. ACC is the spatial correlation of 950 hPa temperature anomalies relative to the August climatology (1981–2010), and RMSE of 950 hPa temperature anomalies is averaged from August 2nd–13th. NeuralGCM prediction averaged from August 2nd–13th of (e) 200 hPa horizontal wind divergence (shading) and geopotential anomaly (contour), (f) 500 hPa specific humidity anomaly, and (g) 500 hPa specific cloud liquid water content (shading) and specific cloud ice water content (contour).

2.2.2. Twenty-Four Regional-Conditioned Sensitivity Experiments

The Northern Hemisphere domain (30°S–90°N, 0°–360°E) is equally partitioned into 24 regions (60° longitude × 30° latitude; Figure 2a). In each sensitivity experiment (denoted as exp-n), all anomalies in the initial conditions of the 37-level inputs and sea surface forcings within a single domain are replaced with their climatological values, and forecast for the subsequent 15 days. The regional impact (RI) of each region is defined as the difference of spatial mean 950 hPa temperature anomaly over the SC domain (104°–122°E, 25°–35°N) between the sensitivity experiment and the control forecast. A bootstrap test with replacement (10,000 resamples), assuming independent samples, is used to assess whether the period-mean RI is significantly different from zero at the 95% confidence level. We also used the IPCC climate reference regions (Iturbide et al., 2020) to test the

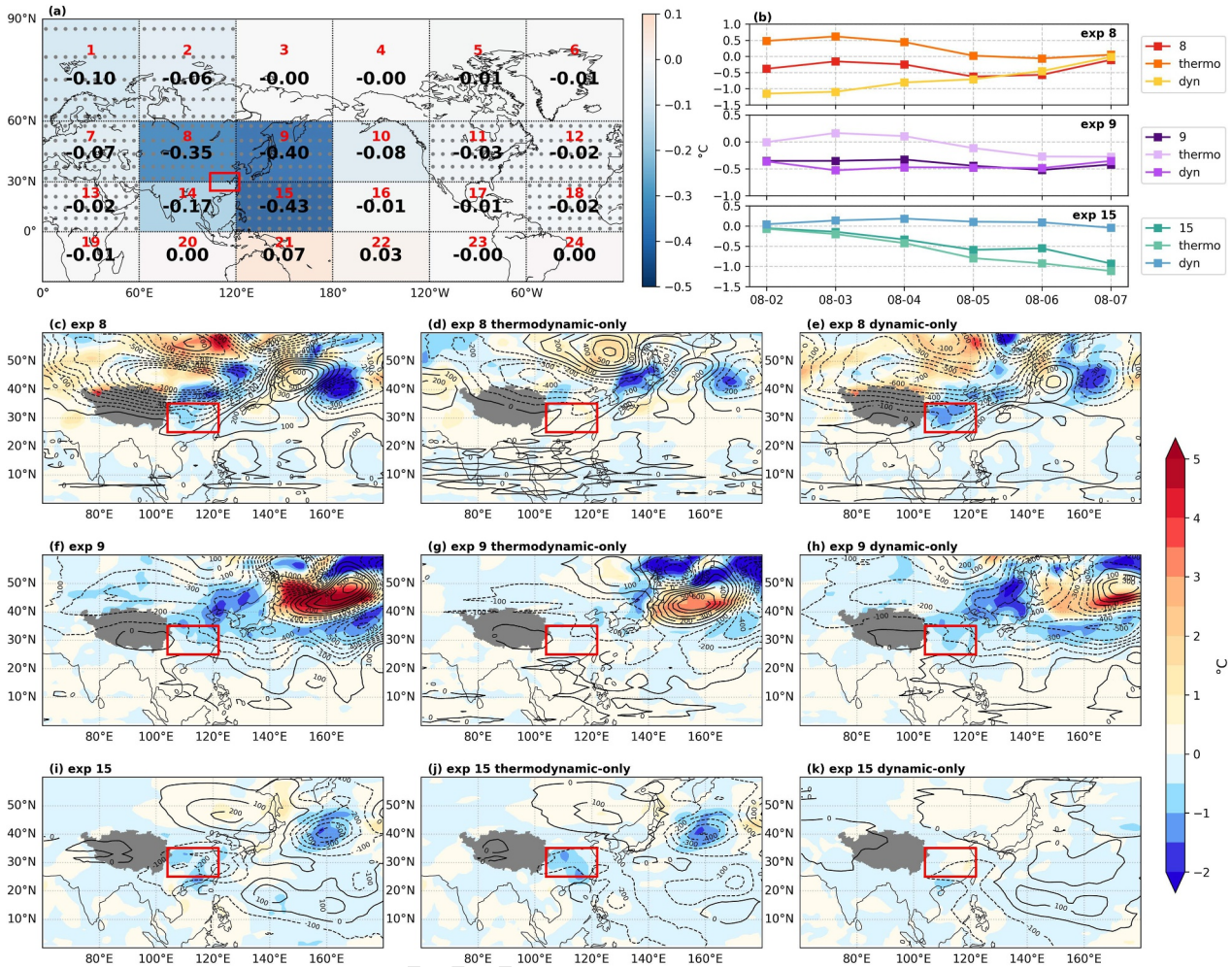

Figure 2. Regional division of 24-grid sensitivity experiments and the impact to SCH22 from adjacent regions in 0–5 days (a) Region division (red text: numbering) and their RI (black text, °C) on SC (red box) averaged from August 2nd to 7th (inclusive). Dotted regions indicate exceeding the 95% confidence level. (b) Temporal evolution of RIs (°C) in regional conditioned, dynamic-only, and thermodynamic-only sensitivity experiments (c-k) Maps corresponding to panel (b), of impacts on 950 hPa temperature anomalies (shading) and 200 hPa geopotential anomalies (contours) averaged from August 2nd to 7th.

robustness of our results by accounting for key climate regions (Text S2 and Figures S4 and S5 in Supporting Information S1).

2.2.3. Dynamic and Thermodynamic Decomposition

To isolate dynamic versus thermodynamic contributions in adjacent regions 8, 9, and 15, we conduct two supplemental sets of experiments. In dynamic-only runs, temperature, specific humidity, specific cloud ice water content, and specific cloud liquid water content in the initial conditions are set to climatology, while in thermodynamic-only runs, horizontal winds and geopotential in the initial conditions were set to climatology at initialization, to make the forecast as in the control prediction. It should be noted here that we separate the dynamical and thermodynamical processes solely in the sense of their effect from initialization only. No changes in the actual model are made.

2.2.4. Forecast With Only HIRs

High impact regions (HIRs) of SCH22 are defined as regions that have significant impact on the temperature anomalies of SC. To confirm the decisive impact of HIRs on SCH22, we design two additional forecast experiments. For HIRs prediction (Figure 3c), anomalies of initial conditions are restricted in HIRs (local regions 8, 9, 14, and 15, and remote regions 1, 2, 6, 11, and 12), which represent about 25% of the globe, while all the rest of

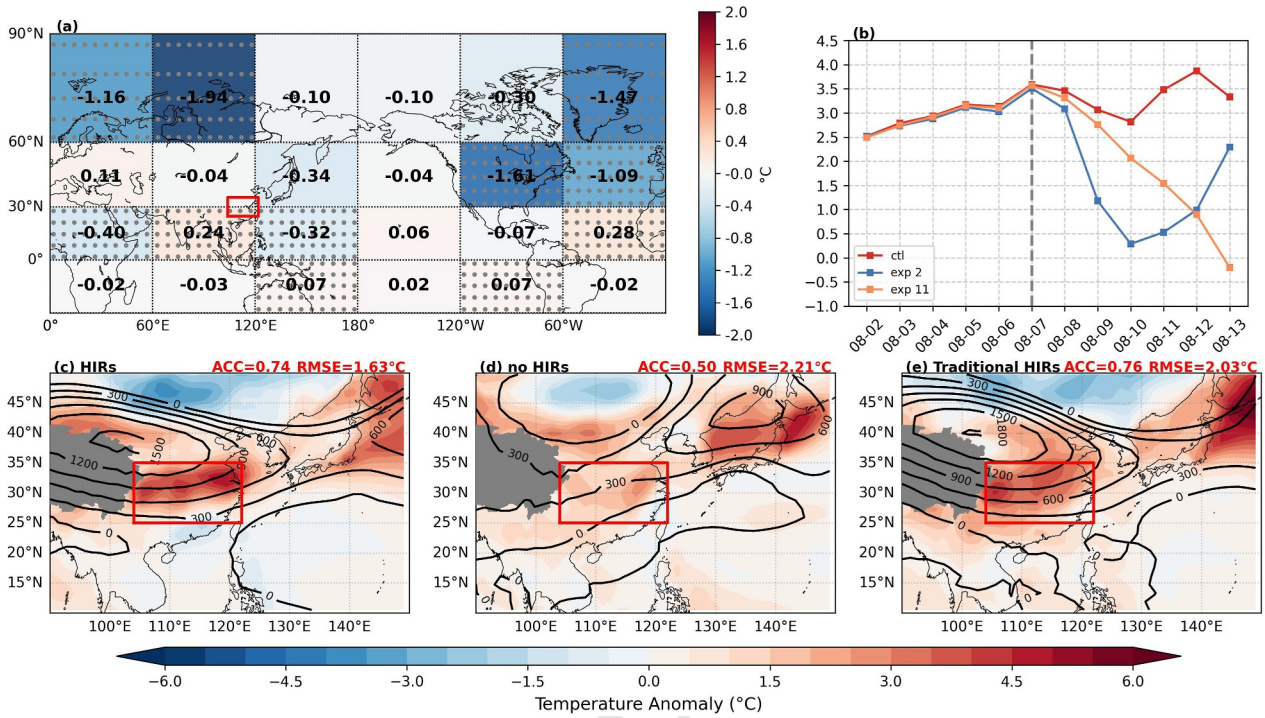

Figure 3. Impact from remote regions to SCH22 in 6–11 days and HIRs/no HIRs predictions. (a) As in Figure 2a, but averaged from August 8th to 13th. (b) Daily temperature anomaly in SC from control prediction (red), removing region 2 (blue), and region 11 (orange) from August 2nd to 13th. (c–e) The same as in Figure 1d, but predicted from initial anomalies of (c) HIRs (adjacent regions 8, 9, 14, and 15, and remote regions 1, 2, 6, 11, and 12); (d) the remaining regions; and (e) HIRs derived from composite analysis. ACC and RMSE are relative to the control prediction. Red box denotes SC region.

the globe is kept climatology. For no-HIRs prediction (Figure 3d), anomalies of initial conditions are eliminated in HIRs, while the rest of the globe keeps initial anomalies.

3. Results

3.1. NeuralGCM Predictions of the 2022 South China Heatwave

Initialized from August 2nd, NeuralGCM skillfully reproduces both ERA5's temporal evolution (Figure 1b) and spatial structure (Figure 1d) of the heatwave. Errors in its daily 950 hPa temperature anomalies remain less than 1°C for the first 10 days of the simulation (Figure 1b), with a spatial anomaly correlation coefficient (ACC) of 0.91 (Figures 1c and 1d) and root-mean-square error (RMSE) of 1.25°C. The model captures a high-pressure anomaly north of the Tibetan Plateau over North and East China, accompanied by anomalous warming centered over North China and a stronger, broader center over East-Central China, in close agreement with observations (Figures 1c and 1d).

In the upper troposphere, strong wind convergence over SC drives robust subsidence (Figure 1e), which would yield anomalously dry conditions below. Although care should be taken in interpreting physical processes from a model whose parametrizations are predominantly statistically learned, our results show that NeuralGCM does appear to reproduce real-world physics remarkably well. The adiabatic subsidence and drying (Figure 1f), for example, does appear to suppress cloud formation and impact the expected cloud-radiative processes, with corresponding reductions in both specific cloud liquid and ice water content (Figure 1g). The resulting decrease in cloud cover would increase the incoming shortwave radiation reaching the surface, further amplifying its warming. The forecast skill of NeuralGCM declines naturally after August 13th due to the absence of oceanic and land-surface coupling.

3.2. Identification of Local Drivers Through Sensitivity Experiments (0–5 Days)

Leveraging NeuralGCM's good predictive ability, we conduct 24 sensitivity experiments to find where are the regions that has the greatest impact on the predicted temperature anomalies over SC. Averaged over the first 0–5 days, regions 8, 9, and 15 clearly induce the greatest RI (−0.35, −0.40, and −0.43°C, respectively; Figure 2a), indicating that early stage heatwave growth is chiefly driven by relatively local, rather than remote, thermodynamic and dynamic processes. A transition of dominant regions from adjacent regions to remote regions can be observed in the daily results (Figures S6a–S6f in Supporting Information S1) on August 7th–8th, which is also consistent among different schemes (Figure S4 in Supporting Information S1), and further confirmed by considering key climate zones following the IPCC climate reference regions (Figure S5 in Supporting Information S1).

Removing these adjacent region initial anomalies also induce negative 200 hPa geopotential anomalies and reduced 950 hPa temperatures (Figures 2c–2i). Specifically, removing anomalies over regions 8 and 9 induces a cyclonic anomaly over North China, extending its influence southwards to East-Central China, resulting in negative temperature anomalies there (Figures 2c and 2f). Similarly, initializing without the observed anomalies over the Northwest Pacific (region 15) generates a cyclonic anomaly from the Yangtze River to SC, and also leads to corresponding cooling (Figure 2i). This highlights that the Northwest Pacific not only modulates seasonal mean conditions but can also influence the synoptic evolution of heatwaves. Further decomposition into "dynamic-only" and "thermodynamic-only" experiments (see Methods) shows that the RI from region 8 is predominantly thermodynamic (Figure 2b, top panel, Figures 2d and 2e), while from region 9, it is initially strongly thermodynamic but then dynamic (Figure 2b, middle panel, Figures 2g and 2h). From region 15, it is mainly dynamic (Figure 2b, bottom panel, Figures 2j and 2k).

3.3. Teleconnected Effects From Remote HIRs (6–11 Days)

At longer lead times (6–11 days), remote teleconnections appear to have dominated the heatwave's development with sequential influences from key remote sectors (Figures S6g–S6l in Supporting Information S1, Figure 3a). Averaged over August 8th–13th, European regions 1 and 2 contribute 1.16°C and 1.94°C to the heatwave, while NA regions 6, 11 and 12 contribute 1.47°C, 1.61°C and 1.09°C (Figure 3a). Figure 3b shows how the initialization of 2 of the 24 experiments can impact the rate of the heatwave's development with time. For these, in which regions 2 and 11, respectively, are initialized from climatology, the heatwave's development stalled after August 7th with the peak associated with local processes, demonstrating the essential role of Europe and NA in the heatwave's growth. A similar phenomenon can also be seen in regions 1, 6, and 12, while impact from other regions is nearly negligible (Figure S7 in Supporting Information S1). More specifically, the European impact appears earlier. Without the initial anomalies in region 2 (blue line in Figure 3b), SC cools sharply after August 7th but warms again on and after 10th, notably coinciding with a change in the control run also on the 10th, suggesting that region 2 has an outsized role in the heatwave during this period. This differs, interestingly, from the cooling impact from NA, which becomes even more prominent after 10th. Together with the earlier findings, these results indicate that the heatwave in SC is strongly influenced by a relay-like sequence of a combination of drivers from local forcings at short leads (0–5 days), European anomalies during intermediate stages (~5–8 days), and NA anomalies during the intensification phase (~8–11 days), reflecting a gradual reorganization of the large-scale atmospheric circulation and the delayed emergence of remote teleconnection influences rather than an abrupt change. Correspondingly, concurrent heatwaves are observed over Europe, SC, and NA both in monthly mean and the initial condition at 0:00 August 2nd, and also follow this sequence on the daily timescale (Figure S2 in Supporting Information S1). Impact from Europe and NA are test robust among different schemes, however, it should be noted here that Tibetan Plateau also showed strong and significant impact when examined in isolation, whose impact may be weakened by the uniform regional division (Figures S5b, S3a, S4b, S4d in Supporting Information S1).

Given the clearly strong roles of the European and NA regions shown above, we now identify these remote HIRs and examine their combined impact on SC. We do this by running two additional global simulations of NeuralGCM: one with the initial conditions maintaining anomalies only in the regions discussed above (the adjacent regions 8, 9, 14, and 15, and the remote regions 1, 2, 6, 11, and 12) and one with the initial conditions maintaining anomalies in the rest of the world. The first gives a prediction (Figure 3c) with an ACC of 0.74 and RMSE of 1.63°C relative to the control run, with the heatwave positioned in an almost identical location, but of slightly

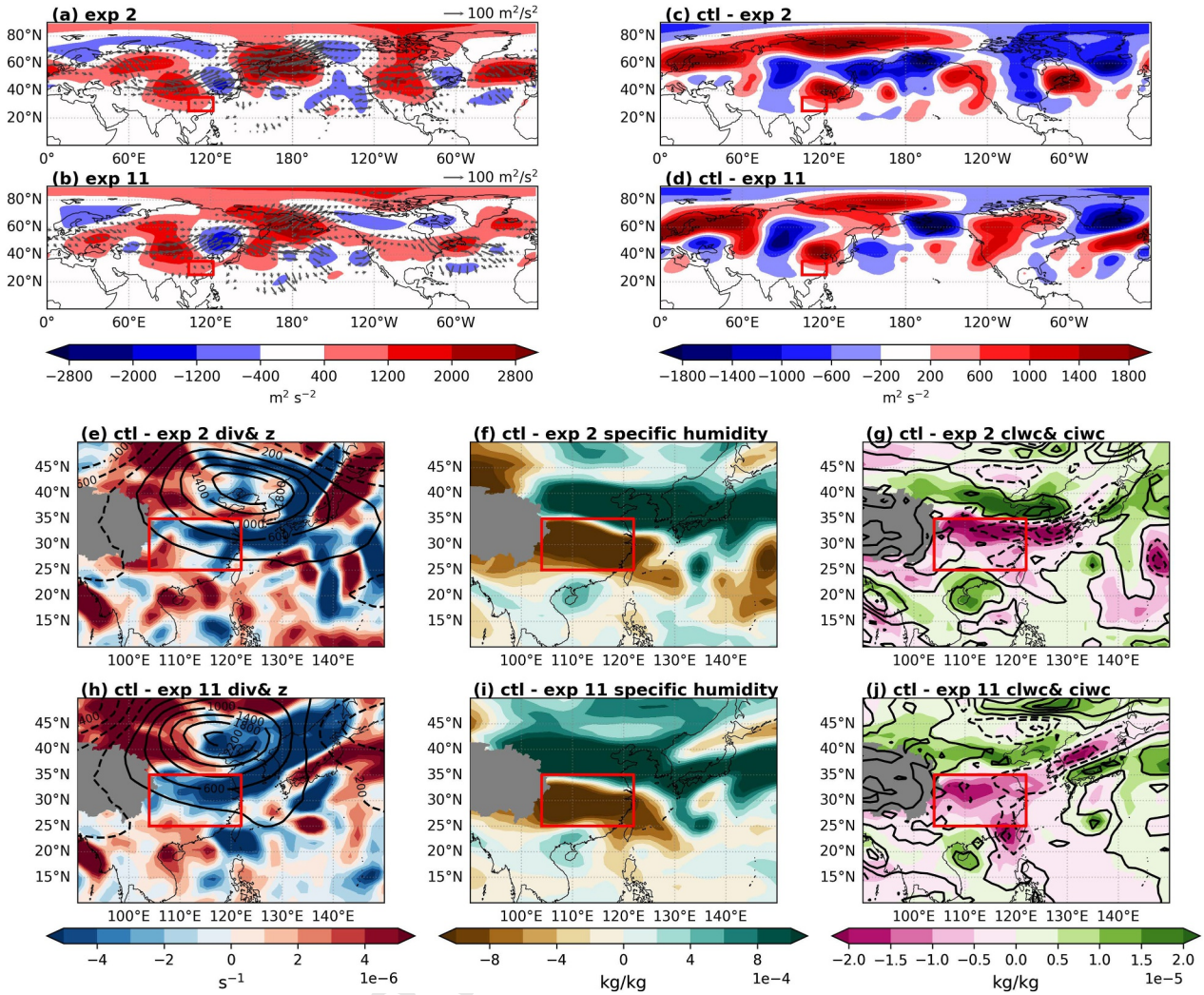

Figure 4. Physical mechanisms linking remote HIRs to SCH22. 200 hPa geopotential anomaly (shading) and T-N wave-activity flux (WAF, Takaya & Nakamura, 2001, Text S3 in Supporting Information S1) (vector) averaged over August 8th–13th of (a) removing region 2, and (b) removing region 11. 200 hPa geopotential anomaly (shading) in control prediction (Figure S10a in Supporting Information S1) minus (c) removing region 2, and (d) removing region 11, respectively. (e–j) Same as in Figures 1e–1g, but averaged over August 8th–13th of (e–g) control prediction minus removing region 2, and (h–j) control prediction minus removing region 11.

reduced amplitude and spatial coverage. This is comparable to the predictions initialized on HIRs identified by composite analysis covering almost the entire globe north of 20°N (Figure 3e). The corresponding geopotential anomaly over Northwest China is also very well reproduced by the new prediction. The prediction skill beyond 0–5 days declines as the initial anomaly field shrinks (Figure S8 in Supporting Information S1). In contrast, the second new prediction fails to capture either the intensity or spatial pattern of the heatwave (Figure 3d). An independent set of experiments (Figure S9 in Supporting Information S1) using the FuXi AI model also gives similar results, indicating that the impacts of the regions mentioned above are robust.

3.4. Synoptic Reasoning

We now turn our attention to examining possible reasons for the strong role that conditions over Europe and NA appeared to play in the SCH22. To do this, we focus again on the two regionally conditioned NeuralGCM runs (2 and 11) that appeared to produce the greatest remote roles in the August 8th–13th part of the heatwave. Figures 4a–4d gives maps of the 200 hPa geopotential anomaly for these as well as their departure from the anomaly given by the control run (Figure S10a in Supporting Information S1). A very clear wave train spans multiple continents (Figures 4a–4d, Figure S10 in Supporting Information S1), whose energy generally

propagates to the east with influences on the SC region from the northwest. A similar phenomenon can also be seen in regions 1, 6, and 12 (Figure S11 in Supporting Information S1).

Comparing the wave train anomalies of these two runs with those (not shown) of the other 22 regionally conditioned runs suggests that anomalies over both Europe and NA worked in tandem to excite a wave-like pattern, supporting the formation of the anti-cyclonic anomaly over eastern Asia (Figures 4a and 4b). Compared to the control run, the two shown in Figures 4a and 4b also exhibit strong upper-level convergence centered northeast of SC, together with negative specific humidity anomalies and reductions in cloud liquid and ice water content (Figures 4e–4j). These local feedbacks also mirror those seen in the full reforecast experiments (Figures 1e–1g) and demonstrate how teleconnection-induced circulation patterns excited by anomalies in specific regions can directly support the development of heatwaves in SC. Simulations with the FuXi model yield nearly identical results (Figure S12 in Supporting Information S1), underscoring the robustness of our framework.

4. Summary and Discussion

Using a cost-effective hybrid dynamical-machine learning weather model NeuralGCM, we present an AI enabled framework designed to easily identify which regions of the world had the greatest influence on the development of an extreme heatwave in SC in August 2022. We have illustrated that local thermodynamic and dynamic processes played the greatest role early stage (0–5 days), consistent with prior case studies emphasizing local land-atmosphere interactions (Gong et al., 2024; Ma et al., 2024). Influences from as far afield as Europe and NA, however, played an outsized role in prolonging the extreme conditions. By defining these key regions as HIRs, we show that forecasts initialized using anomalies only from these HIRs, which cover just 25% of the global domain, successfully reproduce the evolution and spatial pattern of the heatwave.

These findings complement observational analyses and GCM experiments linking circumglobal wave trains to synchronized extremes (Barriopedro et al., 2023; Ding & Wang, 2005; Kornhuber et al., 2019; Rogers et al., 2022; Saeed et al., 2014; Wang et al., 2017), and uniquely provide a predictive, event-specific detection of precursors and quantification of remote influences. Our diagnosing approach can serve as an additional method compared to studies based on the predicting limitation (Vonich & Hakim, 2024), showing potential for AI model evaluation and improving forecast. We hope that this diagnostic framework can be generalized to other heatwave studies and further contribute to an improved understanding of heatwave-related compound extreme events and their adaptation strategies (Tripathy et al., 2023).

Despite these promising advances, some limitations do remain. Although NeuralGCM is test reliable to replicate extreme events (Jiménez-Esteve et al., 2025; Meng et al., 2026), it does not yet incorporate fully coupled ocean, land, and atmosphere processes, which may underestimate feedbacks operating at subseasonal to seasonal timescales or overlook interactions with sea ice and large-scale modes such as the Madden-Julian Oscillation (Coumou et al., 2018; Matsueda & Takaya, 2015; Zhang et al., 2020). Extending this framework with coupled ocean-land models and higher-resolution physics could improve the representation of these processes. This framework is also limited to diagnosing synoptic-scale extreme events due to the ability that AI weather forecast model used in this study can only provide reliable forecast for up to 15 days, and still depends on the selection of initial conditions from reanalysis. The 1.4° deterministic model checkpoints lacks a representation of forecast uncertainty compared to stochastic model or ensemble forecast. Additional work is required to address this limitation, which may bias the magnitude of the RI and potentially alter the ranking among HIRs, however, the HIRs are robustly confirmed by dynamical analysis. And the current uniform regional division may weaken the influence of some small but dynamically important areas like the Tibetan Plateau. Our goal is to provide a rapid and efficient diagnostic for an existing extreme by identifying the regions most responsible for its development, rather than locating where initial perturbations take place can make it most likely to happen, which is the aim of seeking optimal perturbations. Future work remains to learn from nonlinear dynamical methods like the conditional nonlinear optimal perturbation (CNOP) method (Duan et al., 2023; Mu et al., 2003) to improve early warning skill for vulnerable areas and help guide the design of adaptive climate strategies in a warming world.

Conflict of Interest

The authors declare no conflicts of interest relevant to this study.

Availability Statement

ERA5 hourly averaged data on pressure levels is available at Hersbach et al. (2023a), and ERA5 monthly averaged data on pressure levels is available at Hersbach et al. (2023b). Prediction data of this paper are available via a data repository at Xiang (2025).

Acknowledgments
This work was supported by the National Natural Science Foundation of China (Grants 42141019, 42175049, and 42261144687) and the Second Tibetan Plateau Scientific Expedition and Research (STEP) program (Grant. 2019QZKK0102). Contributions from Robin Clark were funded by the Met Office Climate Science for Service Partnership (CSSP) China project under the International Science Partnerships Fund (ISPF).

References

Barriopedro, D., García-Herrera, R., Ordóñez, C., Miralles, D. G., & Salcedo-Sanz, S. (2023). Heat waves: Physical understanding and scientific challenges. *Reviews of Geophysics*, *61*(2), e2022RG000780. https://doi.org/10.1029/2022RG000780

Bellprat, O., Guemas, V., Doblas-Reyes, F., & Donat, M. G. (2019). Towards reliable extreme weather and climate event attribution. *Nature Communications*, *10*(1), 1732. https://doi.org/10.1038/s41467-019-09729-2

Blanchard-Wrigglesworth, E., Cox, T., Espinosa, Z. I., & Donohoe, A. (2023). The largest ever recorded heatwave—Characteristics and attribution of the Antarctic heatwave of March 2022. *Geophysical Research Letters*, *50*(17), e2023GL104910. https://doi.org/10.1029/2023GL104910

Boers, N., Goswami, B., Rheinwalt, A., Bookhagen, B., Hoskins, B., & Kurths, J. (2019). Complex networks reveal global pattern of extreme-rainfall teleconnections. *Nature*, *566*(7744), 373–377. https://doi.org/10.1038/s41586-018-0872-x

Chen, L., Zhong, X., Zhang, F., Cheng, Y., Xu, Y., Qi, Y., & Li, H. (2023). FuXi: A cascade machine learning forecasting system for 15-day global weather forecast. *npj Climate and Atmospheric Science*, *6*(1), 1–11. https://doi.org/10.1038/s41612-023-00512-1

Coumou, D., Di Capua, G., Vavrus, S., Wang, L., & Wang, S. (2018). The influence of Arctic amplification on mid-latitude summer circulation. *Nature Communications*, *9*(1), 2959. https://doi.org/10.1038/s41467-018-05256-8

Di Capua, G., Sparrow, S., Kornhuber, K., Rousi, E., Osprey, S., Wallom, D., et al. (2021). Drivers behind the summer 2010 wave train leading to Russian heatwave and Pakistan flooding. *npj Climate and Atmospheric Science*, *4*(1), 1–14. https://doi.org/10.1038/s41612-021-00211-9

Ding, Q., & Wang, B. (2005). Circumglobal teleconnection in the Northern Hemisphere summer. *Journal of Climate*, *18*(17), 3483–3505. https://doi.org/10.1175/JCLI3473.1

Domeisen, D. I. V., Eltahir, E. A. B., Fischer, E. M., Knutti, R., Perkins-Kirkpatrick, S. E., Schär, C., et al. (2023). Prediction and projection of heatwaves. *Nature Reviews Earth and Environment*, *4*(1), 36–50. https://doi.org/10.1038/s43017-022-00371-z

Dong, S., Sun, Y., Li, C., Zhang, X., Min, S.-K., & Kim, Y.-H. (2021). Attribution of extreme precipitation with updated observations and CMIP6 simulations. *Journal of Climate*, *34*(3), 871–881. https://doi.org/10.1175/JCLI-D-19-1017.1

Duan, W., Yang, L., Mu, M., Wang, B., Shen, X., Meng, Z., & Ding, R. (2023). Recent advances in China on the predictability of weather and climate. *Advances in Atmospheric Sciences*, *40*(8), 1521–1547. https://doi.org/10.1007/s00376-023-2334-0

Fu, Z.-H., Zhou, W., Xie, S.-P., Zhang, R., & Wang, X. (2024). Dynamic pathway linking Pakistan flooding to East Asian heatwaves. *Science Advances*, *10*(17), eadk9250. https://doi.org/10.1126/sciadv.adk9250

Gong, H., Ma, K., Hu, Z., Dong, Z., Ma, Y., Chen, W., et al. (2024). Attribution of the August 2022 extreme heatwave in Southern China: Role of dynamical and thermodynamical processes. *Bulletin of the American Meteorological Society*, *105*(1), E193–E199. https://doi.org/10.1175/bams-d-23-0175.1

Hai, Z., & Perlman, R. L. (2022). Extreme weather events and the politics of climate change attribution. *Science Advances*, *8*(36), eabo2190. https://doi.org/10.1126/sciadv.abo2190

Hersbach, H., Bell, B., Berrisford, P., Biavati, G., Horányi, A., Muñoz Sabater, J., et al. (2023a). ERA5 hourly data on pressure levels from 1940 to present [Dataset]. *Copernicus Climate Change Service (C3S) Climate Data Store (CDS)*. https://doi.org/10.24381/cds.bd0915c6

Hersbach, H., Bell, B., Berrisford, P., Biavati, G., Horányi, A., Muñoz Sabater, J., et al. (2023b). ERA5 monthly averaged data on pressure levels from 1940 to present [Dataset]. *Copernicus Climate Change Service (C3S) Climate Data Store (CDS)*. https://doi.org/10.24381/cds.6860a573

Iturbide, M., Gutiérrez, J. M., Alves, L. M., Bedia, J., Cerezo-Mota, R., Cimadevilla, E., et al. (2020). An update of IPCC climate reference regions for subcontinental analysis of climate model data: Definition and aggregated datasets. *Earth System Science Data*, *12*(4), 2959–2970. https://doi.org/10.5194/essd-12-2959-2020

Jiang, J., Liu, Y., Mao, J., & Wu, G. (2023). Extreme heatwave over Eastern China in summer 2022: The role of three oceans and local soil moisture feedback. *Environmental Research Letters*, *18*(4), 044025. https://doi.org/10.1088/1748-9326/acc5fb

Jiménez-Esteve, B., Barriopedro, D., Johnson, J. E., & García-Herrera, R. (2025). AI-driven weather forecasts to accelerate climate change attribution of heatwaves. *Earth's Future*, *13*(8), e2025EF006453. https://doi.org/10.1029/2025EF006453

Kochkov, D., Yuval, J., Langmore, I., Norgaard, P., Smith, J., Mooers, G., et al. (2024). Neural general circulation models for weather and climate. *Nature*, *632*(8027), 1060–1066. https://doi.org/10.1038/s41586-024-07744-y

Kornhuber, K., Osprey, S., Coumou, D., Petri, S., Petoukhov, V., Rahmstorf, S., & Gray, L. (2019). Extreme weather events in early summer 2018 connected by a recurrent hemispheric wave-7 pattern. *Environmental Research Letters*, *14*(5), 054002. https://doi.org/10.1088/1748-9326/ab13bf

Leach, N. J., Weisheimer, A., Allen, M. R., & Palmer, T. (2021). Forecast-based attribution of a winter heatwave within the limit of predictability. *Proceedings of the National Academy of Sciences*, *118*(49), e2112087118. (world). https://doi.org/10.1073/pnas.2112087118

Liang, X.-Z. (2022). Extreme rainfall slows the global economy. *Nature*, *601*(7892), 193–194. https://doi.org/10.1038/d41586-021-03783-x

Lin, H., Mo, R., & Vitart, F. (2022). The 2021 Western North American heatwave and its subseasonal predictions. *Geophysical Research Letters*, *49*(6), e2021GL097036. https://doi.org/10.1029/2021GL097036

Lu, G., Li, Q., Zhao, M., Dong, L., Wang, L., Zhao, L., et al. (2024). Comparative analysis of peak-summer heatwaves in the Yangtze-Huaihe River Basin of China in 2022 and 2013: Thermal effects of the Tibetan Plateau, *300*, 107222. https://doi.org/10.1016/j.atmosres.2024.107222

Ma, K., Gong, H., Wang, L., Liu, B., Li, Y., Ran, H., & Chen, W. (2024). Anthropogenic forcing intensified internally driven concurrent heatwaves in August 2022 across the Northern Hemisphere. *npj Climate and Atmospheric Science*, *7*(1), 290. https://doi.org/10.1038/s41612-024-00828-6

Ma, Y.-Y., Chen, Y.-T., Hu, X.-X., Ma, Q.-R., Feng, T.-C., Feng, G.-L., & Ma, D. (2023). The 2022 record-breaking high temperature in China: Sub-seasonal stepwise enhanced characteristics, possible causes and its predictability. *Advances in Climate Change Research*, *14*(5), 651–659. https://doi.org/10.1016/j.accre.2023.09.008

Mallapaty, S. (2022). China's extreme weather challenges scientists studying it. *Nature*, *609*(7929), 888. https://doi.org/10.1038/d41586-022-02954-8

Matsueda, S., & Takaya, Y. (2015). The global influence of the Madden–Julian Oscillation on extreme temperature events. *Journal of Climate*, *28*(10), 4141–4151. https://doi.org/10.1175/JCLI-D-14-00625.1

Meng, Z., Hakim, G. J., Yang, W., & Vecchi, G. A. (2026). Deep learning atmospheric models reliably simulate out-of-sample land heat and cold wave frequencies. *Geophysical Research Letters*, *53*(3), e2025GL117990. https://doi.org/10.1029/2025GL117990

Mora, C., Dousset, B., Caldwell, I. R., Powell, F. E., Geronimo, R. C., Bielecki, C. R., et al. (2017). Global risk of deadly heat. *Nature Climate Change*, *7*(7), 501–506. https://doi.org/10.1038/nclimate3322

Mu, M., Duan, W. S., & Wang, B. (2003). Conditional nonlinear optimal perturbation and its applications. *Nonlinear Processes in Geophysics*, *10*(6), 493–501. https://doi.org/10.5194/npg-10-493-2003

Newman, R., & Noy, I. (2023). The global costs of extreme weather that are attributable to climate change. *Nature Communications*, *14*(1), 6103. https://doi.org/10.1038/s41467-023-41888-1

Patricola, C. M., & Wehner, M. F. (2018). Anthropogenic influences on major tropical cyclone events. *Nature*, *563*(7731), 339–346. https://doi.org/10.1038/s41586-018-0673-2

Pyrina, M., & Domeisen, D. I. V. (2023). Subseasonal predictability of onset, duration, and intensity of European heat extremes. *Quarterly Journal of the Royal Meteorological Society*, *149*(750), 84–101. https://doi.org/10.1002/qj.4394

Rogers, C. D. W., Kornhuber, K., Perkins-Kirkpatrick, S. E., Loikith, P. C., & Singh, D. (2022). Sixfold increase in historical Northern Hemisphere concurrent large heatwaves driven by warming and changing atmospheric circulations. *Journal of Climate*, *35*(3), 1063–1078. https://doi.org/10.1175/JCLI-D-21-0200.1

Saeed, S., Van Lipzig, N., Müller, W. A., Saeed, F., & Zanchettin, D. (2014). Influence of the circumglobal wave-train on European summer precipitation. *Climate Dynamics*, *43*(1), 503–515. https://doi.org/10.1007/s00382-013-1871-0

Seneviratne, S. I., Zhang, X., Adnan, M., Badi, W., Dereczynski, C., Di Luca, A., et al. (2023). Weather and climate extreme events in a changing climate. In V. Masson-Delmotte, P. Zhai, A. Pirani, S. L. Connors, C. Péan, S. Berger, et al. (Eds.), *Climate change 2021: The physical science Basis. Contribution of Working Group I to the sixth assessment report of the intergovernmental Panel on climate change* (1st ed., pp. 1513–1766). Cambridge University Press. https://doi.org/10.1017/9781009157896.013

Smiley, K. T., Noy, I., Wehner, M. F., Frame, D., Sampson, C. C., & Wing, O. E. J. (2022). Social inequalities in climate change-attributed impacts of Hurricane Harvey. *Nature Communications*, *13*(1), 3418. https://doi.org/10.1038/s41467-022-31056-2

Stott, P. A., Stone, D. A., & Allen, M. R. (2004). Human contribution to the European heatwave of 2003. *Nature*, *432*(7017), 610–614. https://doi.org/10.1038/nature03089

Takaya, K., & Nakamura, H. (2001). A formulation of a phase-independent wave-activity flux for stationary and migratory quasigeostrophic eddies on a zonally varying basic flow. *Journal of the Atmospheric Sciences*, *58*(6), 608–627. https://doi.org/10.1175/1520-0469(2001)058<0608:AFOAPI>2.0.CO;2

Tang, S., Qiao, S., Wang, B., Liu, F., Feng, T., Yang, J., et al. (2023). Linkages of unprecedented 2022 Yangtze River Valley heatwaves to Pakistan flood and triple-dip La Niña. *npj Climate and Atmospheric Science*, *6*(1), 44. https://doi.org/10.1038/s41612-023-00386-3

Thompson, V., Mitchell, D., Hegerl, G. C., Collins, M., Leach, N. J., & Slingo, J. M. (2023). The most at-risk regions in the world for high-impact heatwaves. *Nature Communications*, *14*(1), 2152. https://doi.org/10.1038/s41467-023-37554-1

Touma, D., Stevenson, S., Lehner, F., & Coats, S. (2021). Human-driven greenhouse gas and aerosol emissions cause distinct regional impacts on extreme fire weather. *Nature Communications*, *12*(1), 212. https://doi.org/10.1038/s41467-020-20570-w

Tradowsky, J. S., Bodeker, G. E., Noble, C. J., Stone, D. A., Rye, G. D., Bird, L. J., et al. (2023). A forecast-model-based extreme weather event attribution system developed for Aotearoa New Zealand. *Environmental Research: Climate*, *2*(4), 045008. https://doi.org/10.1088/2752-5295/acf4b4

Tripathy, K. P., Mukherjee, S., Mishra, A. K., Mann, M. E., & Williams, A. P. (2023). Climate change will accelerate the high-end risk of compound drought and heatwave events. *Proceedings of the National Academy of Sciences*, *120*(28), e2219825120. https://doi.org/10.1073/pnas.2219825120

Vonich, P. T., & Hakim, G. J. (2024). Predictability limit of the 2021 Pacific Northwest heatwave from deep-learning sensitivity analysis. *Geophysical Research Letters*, *51*(19), e2024GL110651. https://doi.org/10.1029/2024GL110651

Wang, J., Chen, Y., Liao, W., He, G., Tett, S. F. B., Yan, Z., et al. (2021). Anthropogenic emissions and urbanization increase risk of compound hot extremes in cities. *Nature Climate Change*, *11*(12), 1084–1089. https://doi.org/10.1038/s41558-021-01196-2

Wang, P., Tang, J., Sun, X., Wang, S., Wu, J., Dong, X., & Fang, J. (2017). Heat waves in China: Definitions, leading patterns, and connections to large-scale atmospheric circulation and SSTs. *Journal of Geophysical Research: Atmospheres*, *122*(20), 10679–10699. https://doi.org/10.1002/2017JD027180

Wang, Z., Luo, H., & Yang, S. (2023). Different mechanisms for the extremely hot central-eastern China in July–August 2022 from a Eurasian large-scale circulation perspective. *Environmental Research Letters*, *18*(2), 024023. https://doi.org/10.1088/1748-9326/acb3e5

Xiang, L. (2025). Revealing the mechanisms of heat extremes using an AI enabled diagnostic framework [Dataset]. *Zenodo*. https://doi.org/10.5281/zenodo.17810636

Xu, F., & Liang, X. S. (2020). The synchronization between the zonal jet stream and temperature anomalies leads to an extremely freezing North America in January 2019. *Geophysical Research Letters*, *47*(19), e2020GL089689. https://doi.org/10.1029/2020GL089689

Zhang, L., Yu, X., Zhou, T., Zhang, W., Hu, S., & Clark, R. (2023). Understanding and attribution of extreme heat and drought events in 2022: Current situation and future challenges. *Advances in Atmospheric Sciences*, *40*(11), 1941–1951. https://doi.org/10.1007/s00376-023-3171-x

Zhang, R., Sun, C., Zhu, J., Zhang, R., & Li, W. (2020). Increased European heat waves in recent decades in response to shrinking Arctic sea ice and Eurasian snow cover. *npj Climate and Atmospheric Science*, *3*(1), 7. https://doi.org/10.1038/s41612-020-0110-8

Zhang, W., Zhou, T., & Wu, P. (2024). Anthropogenic amplification of precipitation variability over the past century. *Science*, *385*(6707), 427–432. https://doi.org/10.1126/science.adp0212

Zheng, J., & Wang, C. (2021). Influences of three oceans on record-breaking rainfall over the Yangtze River Valley in June 2020. *Science China Earth Sciences*, *64*(10), 1607–1618. https://doi.org/10.1007/s11430-020-9758-9